

GCT: Graph Co-Training for Semi-Supervised Few-Shot Learning

Rui Xu[†], Lei Xing[†], Shuai Shao, Lifei Zhao, Baodi Liu*, Member, IEEE, Weifeng Liu*, Senior Member, IEEE, and Yicong Zhou, Senior Member, IEEE

Abstract—Few-shot learning (FSL), purposing to resolve the problem of data-scarce, has attracted considerable attention in recent years. A popular FSL framework contains two phases: (i) the pre-train phase employs the base data to train a CNN-based feature extractor. (ii) the meta-test phase applies the frozen feature extractor to novel data (novel data has different categories from base data) and designs a classifier for recognition. To correct few-shot data distribution, researchers propose Semi-Supervised Few-Shot Learning (SSFSL) by introducing unlabeled data. Although SSFSL has been proved to achieve outstanding performances in the FSL community, there still exists a fundamental problem: the pre-trained feature extractor can not adapt to the novel data flawlessly due to the cross-category setting. Usually, large amounts of noises are introduced to the novel feature. We dub it as Feature-Extractor-Maladaptive (FEM) problem. To tackle FEM, we make two efforts in this paper. First, we propose a novel label prediction method, Isolated Graph Learning (IGL). IGL introduces the Laplacian operator to encode the raw data to graph space, which helps reduce the dependence on features when classifying, and then project graph representation to label space for prediction. The key point is that: IGL can weaken the negative influence of noise from the feature representation perspective, and is also flexible to independently complete training and testing procedures, which is suitable for SSFSL. Second, we propose Graph Co-Training (GCT) to tackle this challenge from a multi-modal fusion perspective by extending the proposed IGL to the co-training framework. GCT is a semi-supervised method that exploits the unlabeled samples with two modal features to crossly strengthen the IGL classifier. We estimate our method on five benchmark few-shot learning datasets and achieve outstanding performances compared with other state-of-the-art methods. It demonstrates the effectiveness of our GCT.

Index Terms—Few-shot learning, Semi-Supervised Few-Shot Learning (SSFSL), Feature-Extractor-Maladaptive (FEM), Isolated Graph Learning (IGL), Graph Co-Training (GCT).

I. INTRODUCTION

In recent years, the performance of computer vision tasks based on deep learning has reached or even surpassed the human beings' level, such as image classification [1]–[3], person re-identification [4]–[6], and point cloud recognition

Rui Xu, Shuai Shao, Baodi Liu, and Weifeng Liu are with the College of Control Science and Engineering, China University of Petroleum (East China), Qingdao, 266580, China. Rui Xu is also with the Yunnan Key Laboratory of Media Convergence, Kunming, 650000, China. Shuai Shao is also with the Zhejiang Lab, Hangzhou, 311100, China. Lei Xing and Lifei Zhao are with the College of Oceanography and Space Informatics, China University of Petroleum (East China), Qingdao, 266580, China. Yicong Zhou is with Department of Computer and Information Science, Faculty of Science and Technology, University of Macau.

[†]Rui Xu and Lei Xing are co-first authors.

*Baodi Liu (Email: thu.liubaodi@gmail.com) and Weifeng Liu (Email: liuwf@upc.edu.cn) are corresponding authors.

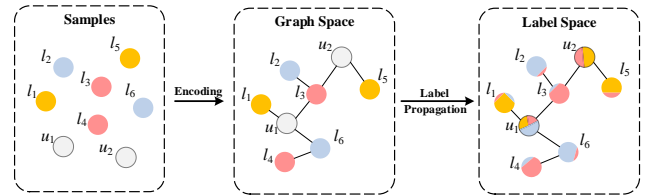


Fig. 1: Isolated Graph Learning (IGL) classifier. $l.$ and $u.$ denote the labeled and unlabeled samples, respectively. IGL first encodes the samples to graph representation and then propagate the label information through graph structure for prediction.

[7]–[9]. The adequate labeled data plays a crucial role for the success. However, it is a challenge for data collection and maintenance in real-world situations. To this end, few-shot learning (FSL), as a pioneer work to address the lack of labeled samples for each category, has aroused widespread concerns.

In a standard FSL, the employed data includes two parts, *i.e.*, base set and novel set. There are many labeled samples in the base set, but very few in the novel set (typically, for the general FSL setting, each category only has 1 or 5 labeled samples). Notably, the categories contained in the base set are entirely different from those in the novel set. Generally, researchers split the FSL model into two phases: (i) pre-train. Training a feature extractor through the base set. (ii) meta-test. First, employing the feature extractor to extract the features of novel data, and then designing a classifier to recognize the novel data's category. Besides, to overcome overfitting caused by the *few-shot* setting, researchers prefer to decouple the complete model, that is, freezing the parameters of the feature extractor after pre-training and directly extracting the cross-category novel features in the meta-test phase.

During the the stage of designing the classifier, the FSL-based methods can be categorized into two sorts according to the type of data employed: (i) supervised FSL, and (ii) semi-supervised FSL. Specifically, the novel data includes three components: support data (*i.e.*, labeled training data), unlabeled data (*i.e.*, unlabeled training data), and query data (*i.e.*, to-be-classified testing data). The difference between the two settings is whether to use the unlabeled data when building the classifier. For more details, please see Section III.

Compared with the supervised FSL, semi-supervised approaches [10]–[13] can effectively correct few-shot data distributions to make the learned classifiers have higher quality.

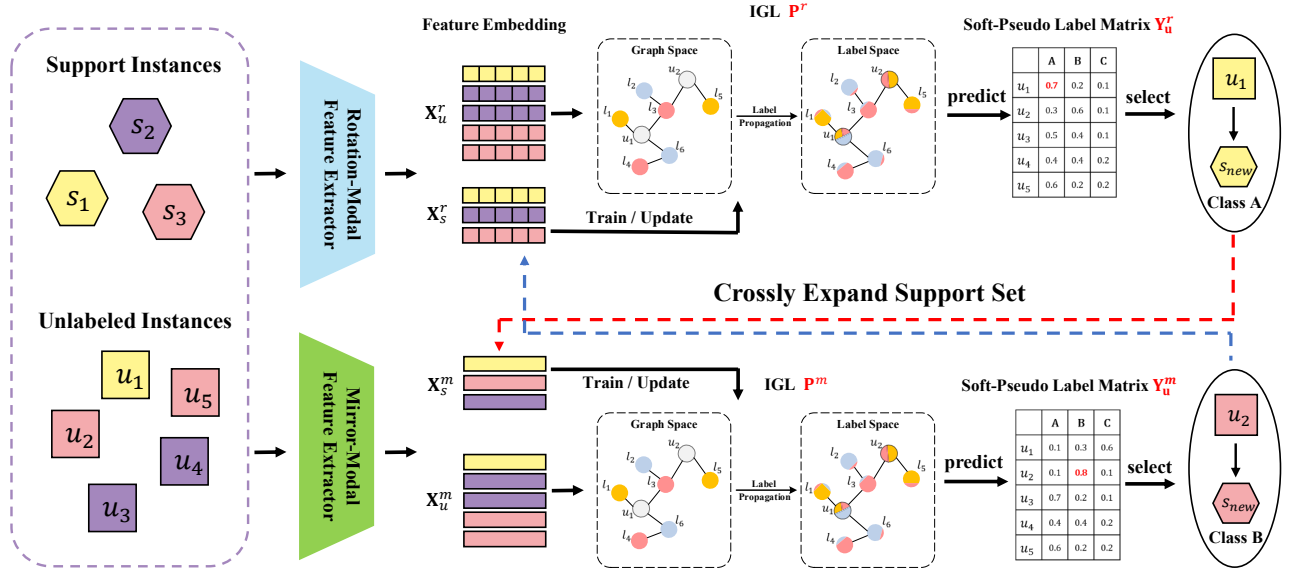


Fig. 2: The flowchart of Graph Co-Training (GCT) in inductive semi-supervised case. We have two kinds of feature extractors, *i.e.*, rotation-modal feature extractor and mirror-modal feature extractor. \mathbf{X}_s^r and \mathbf{X}_s^m indicate the features of support data in rotation-modality and mirror-modality. \mathbf{X}_u^r and \mathbf{X}_u^m represent the features of unlabeled data in corresponding modalities. In each modality, we first employ the support samples to train the basic classifiers \mathbf{P}^r and \mathbf{P}^m (*i.e.*, IGL). Then, we use IGL classifier to predict unlabeled samples and obtain the corresponded soft-pseudo label matrices \mathbf{Y}_u^r and \mathbf{Y}_u^m . Next, we select the most confident sample and give it one-hot-pseudo label. Note that different modalities may predict different results. Finally, we crossly expand the predicted-pseudo-sample to the support set and update the IGL classifier.

However, to achieve this goal, it must be on the premise that sample features are less noisy. But unfortunately, a fundamental problem in FSL, Feature-Extractor-Maladaptive (FEM), is easy to break up the assumption. Specifically, researchers obtain a feature extractor in the pre-train process and apply it directly to the meta-test process, which is challenging to ensure that the frozen feature extractor is capable of adapting to the novel categories. To solve this challenge, we make two efforts in this paper.

First, inspired by [14], we know that transforming the raw data to graph representation is helpful in reducing the dependence on features in classification tasks. To this end, we propose a novel label prediction method dubbed as Isolated Graph Learning (IGL), try to weaken the negative impact of noise from the feature representation perspective. The framework of IGL is shown in Figure 1. We first introduce the graph Laplacian operator to encode the sample's feature embedding to graph space and then project the graph representation to label space for prediction by regularization. Compared with the traditional graph learning method [15], needing both labeled and unlabelled data to propagate label information, our IGL is more flexible to independently complete training and testing procedures. Furthermore, compared with graph neural network (GNN) based methods, there are no abundant parameters in our IGL that need to be updated with the propagation of deep neural networks. In other words, it is easy to be implemented. These attributes are very friendly for few-shot classification in the semi-supervised setting.

Second, we propose Graph Co-Training (GCT) to weaken

the negative effect of noise from a multi-modal fusion perspective. Suppose that we have features from different feature extractors, we can integrate different predictions (obtained from different features) through collaborative training (co-training) to complete the final classification. To be more specific, we first try to get two-modal features from two designed feature extractors. In this phase, we have the flexibility to adapt the classical models in few-shot communities. This paper uses two kinds of self-supervision ways from [16], [17]. Then, we exploit the support data to train two basic classifiers (*i.e.*, IGL) with different modal features. Next, we separately predict the unlabeled data with the two modalities of classifiers. At last, we apply the unlabeled data with the most confident predictions to crossly update the classifiers. The designed co-training way is mainly to strengthen our classifier's robustness to reduce the interference caused by FEM. We illustrate the framework of our GCT in Figure 2. For convenience, we list some crucial abbreviations and notations in Table I.

In summary, the main contributions focus on:

- Aiming at the Feature-Extractor-Maladaptive (FEM) problem in semi-supervised few-shot learning, we propose a novel graph learning based classifier dubbed as Isolated Graph Learning (IGL), which completes training and testing procedures independently.
- We combine our IGL with the co-training framework to design a Graph Co-training (GCT) algorithm. It extends IGL to semi-supervised few-shot learning through fusing multi-modal information.
- The comparison results with SOTAs on five benchmark

TABLE I: The definition of abbreviations and notations.

Abbreviation and Notation	Definition
IGL	Isolated Graph Learning
GCT	Graph Co-Training
FEM	feature-extractor-maladaptive
Std-Mod	standard modality
Meta-Mod	meta modality
SS-R-Mod	self-supervised rotation modality
SS-M-Mod	self-supervised mirror modality
FSL	few-shot learning
ISFSL	inductive supervised few-shot learning
TSFSL	transductive supervised few-shot learning
ISSFSL	inductive semi-supervised few-shot learning
TSSFSL	transductive semi-supervised few-shot learning
$\mathcal{D}_{base}, \mathcal{D}_{novel}$	base data, novel data
$\mathcal{S}, \mathcal{Q}, \mathcal{U}$	support set, query set, unlabeled set
$\omega^r(\cdot), \omega^m(\cdot)$	rotation-modal feature extractor, mirror-modal feature extractor
\mathbf{A}	adjacency matrix
\mathbf{D}	vertex degree matrix
\mathbf{X}	feature embedding of training data
\mathbf{x}_{ts}	feature embedding of testing data
$\mathbf{X}_s^r, \mathbf{X}_s^m$	support feature embedding on rotation-modal and mirror-modal
$\mathbf{X}_u^r, \mathbf{X}_u^m$	unlabeled feature embedding on rotation-modal and mirror-modal
$\mathbf{X}_q^r, \mathbf{X}_q^m$	query feature embedding on rotation-modal and mirror-modal
$\mathbf{x}_{select}^r, \mathbf{x}_{select}^m$	selected the most confidence samples' feature embedding on rotation-modal and mirror-modal
\mathbf{Y}	initial label matrix of training data
$\mathbf{Y}_s^r, \mathbf{Y}_s^m$	one-hot label matrices of support data on rotation-modal and mirror-modal
$\mathbf{Y}_u^r, \mathbf{Y}_u^m$	predicted soft-pseudo label matrices of unlabeled data on rotation-modal and mirror-modal
$\mathbf{Y}_q^r, \mathbf{Y}_q^m$	predicted soft label matrices of query data on rotation-modal and mirror-modal
$\mathbf{y}_{select}^r, \mathbf{y}_{select}^m$	selected the most confidence samples' one-hot-pseudo label vectors on rotation-modal and mirror-modal
\mathbf{P}	classifier
$\mathbf{P}^r, \mathbf{P}^m$	rotation-modal classifier, mirror-modal classifier
$\mathbf{P}_{opt}^r, \mathbf{P}_{opt}^m$	optimal rotation-modal classifier, optimal mirror-modal classifier

FSL datasets have evaluated the efficiency of our GCT.

B. Multi-Modal Few-Shot Learning

II. RELATED WORK

A. Semi-Supervised Few-Shot Learning

Recently, semi-supervised few-shot learning (SSFSL) has attracted lots of attention. Researchers assume that abundant unlabeled data is available to be used for constructing the classifier. They introduce various traditional semi-supervised learning methods to the few-shot learning (FSL) task. Here, we list several classical semi-supervised approaches and corresponding FSL works. (i) Consistency regularization methods aim to improve the robustness of classifiers when the images are noisy. MetaMix [18], BR-ProtoNet [19] *et.al.* promote the classifier from this way. (ii) Self-training methods first train a classifier with labeled data, then exploit it to generate pseudo labels for unlabeled data, and at last update the classifier with pseudo-labeled data. Recent self-training based FSL methods, including LST [10] ICI [11], PLCM [12], iLPC [13] have achieved outstanding performances. (iii) Hybrid based FSL methods, such as MixMatch [20], and FixMatch [21], try to construct a unified framework of semi-supervised learning by combining several current dominant approaches such as self-training and consistency regularization.

As there are two sides to every coin, it is boundedness to define objects from a single point of view. Multi-view learning as an effective strategy has attracted extensive attention in the past decade. In few-shot learning, some similar methods have been proposed, such as: DenseCls [22], its feature map is divided into various blocks, and the corresponding labels are predicted; DivCoop [23] trains the feature extractors on various datasets and integrates them into a multi-domain representation; URT [24] is an improved method compared with DivCoop [23], which proposes a transformer layer to help the network employ various datasets; DWC [25] introduces a cooperate strategy on a designed ensemble model to integrate multiple information. Although the above-mentioned approaches are based on multi-modal learning, they are limited by the fused feature extractors and classifiers. To be more specific, their methods are based on the unified framework, which means that the feature extractors are usually guaranteed to match classifiers in a fixed way. Without this combination, the model performance will be significantly reduced, which greatly limits the scalability of the methods. While our GCT is freed with the feature extractor, thereby is more flexible to be applied in real scenarios.

C. Graph Learning

Graph Learning is an efficient way to model the data correlation of samples, composed of vertex set (*i.e.*, samples) and edge set. Each edge connects two vertices, which is capable of modeling pair-wise relations of samples. Researchers usually employ the adjacency matrix to represent a graph structure. [15] first proposed Graph Learning. In recent years, graph-based neural networks (GNN) have received extensive attention and have developed rapidly. Due to its good performance, GNN-based technologies have been applied in many fields, including few-shot learning [26]–[29], face clustering [30], [31], etc. The former achieves satisfactory performance by cooperating with meta-learning strategy, and the latter designs multiple kinds of GNNs to cooperate with each other to complete goals.

This paper focuses on traditional graph learning. In graph learning, researchers classify the unlabelled data by propagating the label information through graph structure, which is constructed by employing all the data (including labeled and unlabeled data). There are two challenges in the node/graph classification task by using graph learning: (i) In real applications, it is hard to know in advance what the to-be-tested sample looks like. It limits the scenario for this approach. (ii) Leading to a high computational cost. The predicting process is entirely online. All the data must be considered during the learning stage, which results in consuming massive computing resources. Furthermore, researchers have to reconstruct the graph structure to propagate the label information when coming new testing data. This paper proposes a novel method dubbed as Isolated Graph Learning (IGL) to solve this challenge. IGL is a classifier which can be directly applied in the decoupled FSL task.

III. PROBLEM SETUP

In few-shot learning, there exist two processes (*i.e.*, pre-train process and meta-test process) with different categories of samples. Define the base data in pre-train phase as $\mathcal{D}_{base} = \{(x_{(i)}, y_{(i)}) | y_{(i)} \in \mathcal{C}_{base}\}_{i=1}^{N_{base}}$, and the novel data in meta-test phase as $\mathcal{D}_{novel} = \{(x_{(j)}, y_{(j)}) | y_{(j)} \in \mathcal{C}_{novel}\}_{j=1}^{N_{novel}}$, where x and y denote the sample and corresponded label. \mathcal{C}_{base} and \mathcal{C}_{novel} indicate the categories of base data and novel data, $\mathcal{C}_{base} \cap \mathcal{C}_{novel} = \emptyset$. N_{base} and N_{novel} indicate the number of base data and novel data. To overcome overfitting, we follow the decoupled classification setups as [11]. There are three main stages in few-shot learning. First, we use \mathcal{D}_{base} to train a CNN-based feature extractor $\omega(\cdot)$ in the pre-train phase. Second, we freeze the model's parameters and extract the feature embedding of \mathcal{D}_{novel} . Third, we design a classifier for the novel categories' classification.

Specifically, we first define the meta-test dataset as $\mathcal{D}_{novel} = \{\mathcal{S}, \mathcal{Q}, \mathcal{U}\}$, where \mathcal{S} , \mathcal{Q} , and \mathcal{U} indicate support set, query set, and unlabeled set, $\mathcal{S} \cap \mathcal{Q} = \emptyset$, $\mathcal{S} \cap \mathcal{U} = \emptyset$, $\mathcal{Q} \cap \mathcal{U} = \emptyset$. Next, we divide the support, query, and unlabeled sets into different episodes. Each episode has K -way- O -shot samples, where K -way indicates K classes, and O -shot denotes O samples per class. Finally, we employ the to-be-learned classifier to obtain the average classification accuracies of all the meta-test episodes on the query set \mathcal{Q} .

Besides, according to the differences of data used to construct the classifier, we split the few-shot learning into four kinds of settings: (i) inductive supervised few-shot learning (ISFSL), using the support features and labels to train the classifier; (ii) transductive supervised few-shot learning (TSFSL), using the support features, support labels, and query features to train the classifier; (iii) inductive semi-supervised few-shot learning (ISSFSL), using the support features, support labels, and unlabeled features to train the classifier; (iv) transductive semi-supervised few-shot learning (TSSFSL), using the support features, support labels, unlabeled features, and query features to train the classifier.

IV. METHODOLOGY

In this section, we describe our approach in detail. First, we encode the graph structure of samples' relations to the adjacency matrix. Second, we propose a novel graph learning method dubbed as Isolated Graph Learning (IGL) to tackle the FEM to some extent. This strategy introduces the Laplacian operator to transform the samples in feature space to graph representation and then project them to label space for prediction by regularization. Some details are shown in Figure 1. Third, we propose Graph Co-Training (GCT) by expanding the IGL to a co-training framework. GCT is capable of further addressing the FEM problem from a multi-modal fusion perspective. The flowchart is illustrated in Figure 2. At last, we introduce our designed feature extractors in detail.

A. Graph Structure Encoder

A graph can be formulated as $\mathcal{G} = (\mathcal{V}, \mathcal{E})$, where \mathcal{V} and \mathcal{E} represent vertex set and edge set, respectively. In the paper, the vertex set is composed of image samples. We encode the relations between edges and vertices through adjacency matrix $\mathbf{A} \in \mathbb{R}^{|\mathcal{V}| \times |\mathcal{V}|}$. Given the feature embedding of labeled vertices as $\mathbf{X} = [\mathbf{x}_{(1)}, \mathbf{x}_{(2)}, \dots, \mathbf{x}_{(N)}] \in \mathbb{R}^{dim \times N}$, where $\mathbf{x}_{(i)}$, ($i = 1, 2, \dots, N$) indicates the embedding of v_i , and v_i denotes the i -th vertex in \mathcal{V} . dim and N denote the dimension and number of labeled samples. The elements in \mathbf{A} can be defined as:

$$\mathbf{A}_{(i,j)} = \begin{cases} \exp(-dis(\mathbf{x}_{(i)}, \mathbf{x}_{(j)})^2) & \text{if } (v_{(i)}, v_{(j)}) \in e \\ 0 & \text{o.w.} \end{cases} \quad (1)$$

where $(\cdot)_{(i,j)}$ is the (i,j)-element in (\cdot) . e indicates an edge in \mathcal{E} . $dis(\mathbf{x}_{(i)}, \mathbf{x}_{(j)})$ represents the operator to calculate the distance of feature embeddings between $v_{(i)}$ and $v_{(j)}$, in our method, we select the k Nearest Neighbor (KNN) method. Following, we define the vertex degree matrix as $\mathbf{D} \in \mathbb{R}^{N \times N}$, which denotes a diagonal matrix with its (i, i) -element equal to the sum of the i -th row of \mathbf{A} .

B. Isolated Graph Learning

In this section, we propose a novel label prediction method dubbed as Isolated Graph Learning (IGL). IGL is a strategy to solve the FEM problem by transforming the samples in feature space to graph space. Unlike traditional graph learning,

requiring both labeled and unlabelled data to construct the graph, the proposed IGL is more flexible to independently complete training and testing procedures by learning a regularized projection $\mathbf{P} \in \mathbb{R}^{dim \times C}$ to classify different categories. Here, C indicates the total number of classes. We calculate the cost function as:

$$\mathcal{F}(\mathbf{P}) = f_1(\mathbf{P}) + \lambda f_2(\mathbf{P}) + \mu f_3(\mathbf{P}) \quad (2)$$

where λ and μ represent the parameters to balance the function. $f_1(\mathbf{P})$ denotes the graph Laplacian regularizer, which can be formulated as:

$$\begin{aligned} f_1(\mathbf{P}) &= \frac{1}{2} \left(\sum_{i,j=1}^N \mathbf{A}_{(i,j)} \left(\frac{(\mathbf{X}^T \mathbf{P})_{(i,:)}}{\sqrt{\mathbf{D}_{(i,i)}}} - \frac{(\mathbf{X}^T \mathbf{P})_{(j,:)}}{\sqrt{\mathbf{D}_{(j,j)}}} \right)^2 \right) \\ &= \text{tr}(\mathbf{P}^T \mathbf{X} \Delta \mathbf{X}^T \mathbf{P}) \end{aligned} \quad (3)$$

where $(\cdot)_{(i,:)}$ is the i -th row of (\cdot) . $\Delta = \mathbf{D}^{-\frac{1}{2}} \mathbf{A} \mathbf{D}^{-\frac{1}{2}}$ denotes the normalized graph Laplacian operator. $f_2(\mathbf{P})$ indicates the empirical loss term, which can be formulated as:

$$f_2(\mathbf{P}) = \|\mathbf{X}^T \mathbf{P} - \mathbf{Y}\|_F^2 \quad (4)$$

where $\mathbf{Y} \in \mathbb{R}^{N \times C}$ indicates the initial label embedding matrix. For labeled samples, if the i -th sample belongs to the j -th class, $\mathbf{Y}_{(i,j)}$ is 1, and otherwise, it is 0. $f_3(\mathbf{P})$ is the constraint term. In this paper, we introduce $\ell_{2,1}$ -norm to select an essential feature and avoid overfitting for \mathbf{P} , which can be defined as:

$$f_3(\mathbf{P}) = \|\mathbf{P}\|_{\ell_{2,1}} \quad (5)$$

where $\|\cdot\|_{\ell_{2,1}}$ represents $\ell_{2,1}$ -norm of (\cdot) . The objective function on IGL can be formulated as:

$$\begin{aligned} \arg \min_{\mathbf{P}} \mathcal{F}(\mathbf{P}) \\ = \text{tr}(\mathbf{P}^T \mathbf{X} \Delta \mathbf{X}^T \mathbf{P}) + \lambda \|\mathbf{X}^T \mathbf{P} - \mathbf{Y}\|_F^2 + \mu \|\mathbf{P}\|_{\ell_{2,1}} \end{aligned} \quad (6)$$

To optimize this problem, we first relax Equation 6 as:

$$\begin{aligned} \arg \min_{\mathbf{P}, \mathbf{B}} \mathcal{F}(\mathbf{P}, \mathbf{B}) \\ = \text{tr}(\mathbf{P}^T \mathbf{X} \Delta \mathbf{X}^T \mathbf{P}) + \lambda \|\mathbf{X}^T \mathbf{P} - \mathbf{Y}\|_F^2 + \mu \text{tr}(\mathbf{P}^T \mathbf{B} \mathbf{P}) \end{aligned} \quad (7)$$

where \mathbf{B} is a diagonal matrix. Then we alternately update \mathbf{P} and \mathbf{B} until Equation 7 convergence, follow [32], we directly solve the problems as:

$$\mathbf{B}_{(i,i)} = \frac{1}{2 \|\mathbf{P}_{(i,:)}\|_2^2 + 10^{-8}}, \quad i = 1, \dots, \text{dim} \quad (8)$$

$$\mathbf{P} = \mathcal{H}(\mathbf{X}) = \lambda (\mathbf{X} \Delta \mathbf{X}^T + \lambda \mathbf{X} \mathbf{X}^T + \mu \mathbf{B})^{-1} \mathbf{X} \mathbf{Y} \quad (9)$$

Following, given a testing sample embedding $\mathbf{x}_{ts} \in \mathbb{R}^{\text{dim} \times 1}$, we predict the \mathbf{x}_{ts} 's category by:

$$\mathcal{Z}(\mathbf{x}_{ts}) = \text{id}_{\max} \{ \mathbf{x}_{ts}^T \mathbf{P} \} \quad (10)$$

where id_{\max} represents an operator to obtain the index of the max value in the vector.

Algorithm 1: Graph Co-Training for ISSFSL

Input: Base data \mathcal{D}_{base} , novel data \mathcal{D}_{novel}
Output: Query label
1 # pre-train phase
2 Employ \mathcal{D}_{base} to train the rotation-modal feature extractor $\omega^r(\cdot)$ and mirror-modal feature extractor $\omega^m(\cdot)$.
3 # Meta-test phase
4 Extract two-modal feature of \mathcal{D}_{novel} by $\mathbf{X}_{novel}^r = \omega^r(\mathcal{D}_{novel})$, and $\mathbf{X}_{novel}^m = \omega^m(\mathcal{D}_{novel})$.
5 # Co-training steps:
6 Initialize \mathbf{B} and \mathbf{P} .
7 repeat
8 Construct two modal classifiers by Equation 11.
9 Infer pseudo labels and enlarge support data by Equation 12, 13.
10 until the unlabeled data is exhausted.
11 Predict the query labels by Equation 14.

C. Graph Co-Training for Few-Shot Learning

As mentioned in Section III, there exist four kinds of setting in FSL. To make our IGL perform well in all kinds of FSL, we introduce the co-training strategy to further cooperate with IGL, and named the new approach as Graph Co-Training (GCT). On the one hand, it can solve the FEM problem from a multi-modal fusion perspective. For the details of multi-modal information, please refer to Section IV-E. On the other hand, GCT is capable of strengthening the robustness of the to-be-learned classifier by employing the unlabeled data \mathcal{U} . We'll detail how GCT works in the four settings. Notably, both the construction of \mathbf{P} and the collaborative training are designed for each episode.

First see the inductive semi-supervised few-shot learning (ISSFSL). We construct the co-training framework with two modal features, *i.e.*, rotation-modality and mirror-modality. The rotation-modal feature extractor, $\omega^r(\cdot)$ follows [16], the corresponding embeddings of novel data can be defined as $\mathbf{X}_{novel}^r = \omega^r(\mathcal{D}_{novel}) = [\mathbf{X}_s^r, \mathbf{X}_u^r, \mathbf{X}_q^r]$, where $\mathbf{X}_s^r = \omega^r(\mathcal{S})$, $\mathbf{X}_u^r = \omega^r(\mathcal{U})$, and $\mathbf{X}_q^r = \omega^r(\mathcal{Q})$ indicate the features of support, unlabeled, and query data on the rotation-modal. The mirror-modal feature extractor, $\omega^m(\cdot)$ follows [17], the features in this modal are denoted as $\mathbf{X}_{novel}^m = \omega^m(\mathcal{D}_{novel}) = [\mathbf{X}_s^m, \mathbf{X}_u^m, \mathbf{X}_q^m]$. The complete GCT is demonstrated in Figure 2, which consists of four steps:

(i) From Equation 9, we construct two different classifiers \mathbf{P}^r and \mathbf{P}^m by employing two modal support features \mathbf{X}_s^r and \mathbf{X}_s^m , respectively.

$$\begin{cases} \mathbf{P}^r = \mathcal{H}(\mathbf{X}_s^r) \\ \mathbf{P}^m = \mathcal{H}(\mathbf{X}_s^m) \end{cases} \quad (11)$$

(ii) Predict the unlabeled data's label from two modal features by:

$$\begin{cases} \mathbf{Y}_u^r = \mathbf{X}_u^r \mathbf{P}^r \\ \mathbf{Y}_u^m = \mathbf{X}_u^m \mathbf{P}^m \end{cases} \quad (12)$$

where \mathbf{Y}_u^r and \mathbf{Y}_u^m denote predicted **soft-pseudo label matrices** of unlabeled data on rotation-modal and mirror-modal.

(iii) Rank the values in soft-pseudo label matrices, then selecting the most confident unlabeled samples' feature \mathbf{x}_{select}^r and \mathbf{x}_{select}^m on each modal, then asserting them corresponding **one-hot-pseudo label vectors** \mathbf{y}_{select}^r and \mathbf{y}_{select}^m (for more details about how to select the most confident sample, please refer to Section IV-D). Next, crossly extend the pseudo-labeled samples and corresponding labels to the support set on different modals. We formulate this step as:

$$\begin{cases} \mathbf{X}_s^r = [\mathbf{X}_s^r, \mathbf{x}_{select}^r], \mathbf{Y}_s^r = [\mathbf{Y}_s^r, \mathbf{y}_{select}^r] \\ \mathbf{X}_s^m = [\mathbf{X}_s^m, \mathbf{x}_{select}^m], \mathbf{Y}_s^m = [\mathbf{Y}_s^m, \mathbf{y}_{select}^m] \end{cases} \quad (13)$$

where \mathbf{Y}_s^r and \mathbf{Y}_s^m denote the **one-hot label matrices** of support data on two modals.

(iv) Repeat (i), (ii) (iii) until the unlabeled data is exhausted (in the real application, we usually select 80 unlabeled samples, for more discussions and results, please see Section ?? and Figure ??). Then we obtain two optimal classifiers \mathbf{P}_{opt}^r and \mathbf{P}_{opt}^m . Employ them to predict the query labels by:

$$\mathcal{Z}(\mathbf{X}_q^r, \mathbf{X}_q^m) = id_{max} \left\{ \frac{(\mathbf{X}_q^r T \mathbf{P}_{opt}^r + \mathbf{X}_q^m T \mathbf{P}_{opt}^m)}{2} \right\} \quad (14)$$

where $\mathbf{Y}_q^r = \mathbf{X}_q^r T \mathbf{P}_{opt}^r$ and $\mathbf{Y}_q^m = \mathbf{X}_q^m T \mathbf{P}_{opt}^m$, denote the predicted **soft label matrices** of query data on rotation-modality and mirror-modality. We summarize the steps in Algorithm 1.

Next see the transductive semi-supervised few-shot learning (TSSFSL). The query feature is also available when constructing the classifier. Here, we can implement TSSFSL with only a few minor tweaks. Specifically, in step (ii), we have to predict not only unlabeled data but also query data.

Then see the transductive supervised few-shot learning (TSFSL), the unlabeled data is not available, but the query feature is given in advance. Therefore, we just need to replace the unlabeled data with query data in (i)(ii)(iii) steps, and finally classify the query data.

At last see the inductive supervised few-shot learning (ISFSL), the unlabeled data is unavailable, and query data is not given to us in advance. Thus, the co-training strategy can not be used in this case and we think the basic IGL classifier is optimal. We can complete ISFSL by Equation 11 and 14.

D. How to Select the Most Confident Sample?

Here we take the rotation-modal as an example to illustrate the strategy. According to Equation 12, we can get the predicted rotation-model soft label matrix $\mathbf{Y}_u^r \in \mathbb{R}^{N_u \times C}$, where N_u denotes the number of unlabeled samples; C denotes the number of unlabeled categories. For each element $\mathbf{Y}_{u(n,c)}^r$, it means the probability of n -th sample belongs to the c -th category, where $n = 1, 2, \dots, N_u$, $c = 1, 2, \dots, C$. In our strategy, we first traverse all the elements in \mathbf{Y}_u^r to find the largest element, which can be defined as $\mathbf{Y}_{u(n_{max},c_{max})}^r$. The n_{max} -th sample is the to-be-selected most confident sample, which belongs to the c_{max} -th category.

E. Multi-Modal Feature Extractor

We can adopt various modal features from different feature extractors to achieve our purpose. For example: (i) Standard modality (Std-Mod) [11], the feature extractor comes from a standard CNN-based classification structure. (ii) Meta modality (Meta-Mod) [33], the feature extractor combines the strategy of meta-learning with the network. (iii) Self-supervised rotation modality (SS-R-Mod) [16], the feature extractor introduces auxiliary loss to predict the angle of image rotation, including $\{0^\circ, 90^\circ, 180^\circ, 270^\circ\}$. (iv) Self-supervised mirror modality (SS-M-Mod) [17]. Different from the SS-R-Mod, SS-M-Mod introduces another auxiliary loss to predict image mirrors, including $\{vertically, horizontally, diagonally\}$. In most of the experiments, we present the results of collaborative training with SS-R-Mod and SS-M-Mod, and thereby we briefly introduce them.

In the SS-R-Mod, the feature extractor updates the network parameters with two kinds of loss, which are the standard classification loss (*i.e.*, \mathcal{L}^s) and rotation-based self-supervised auxiliary loss (*i.e.*, \mathcal{L}^r). To be more specific, assume there's a base image feature vector \mathbf{x} . We project it into a label space, *i.e.*, $\mathbf{x} \rightarrow \mathbf{z}^s$, where $\mathbf{z}^s = [z_1^s, z_2^s, \dots, z_{C_{base}}^s] \in \mathbb{R}^{C_{base}}$, C_{base} denotes the number of the base category. Then transform it to the probability distribution and calculate the standard classification loss \mathcal{L}^s by cross-entropy function:

$$\mathcal{L}^s = - \sum_{c=1}^{C_{base}} \hat{y}_c^s \log(y_c^s) \quad (15)$$

where $y_c^s = \frac{e^{z_c^s}}{\sum_{c=1}^{C_{base}} e^{z_c^s}}$ indicates the predicted probability that sample \mathbf{x} belongs to class c , while \hat{y}_c^s denotes the groundtruth probability. After that, we map the \mathbf{x} to rotation-based label space, *i.e.*, $\mathbf{x} \rightarrow \mathbf{z}^r$, where $\mathbf{z}^r = [z_1^r, z_2^r, z_3^r, z_4^r] \in \mathbb{R}^4$. We can get the auxiliary loss by:

$$\mathcal{L}^r = - \sum_{c=1}^4 \hat{y}_c^r \log(y_c^r) \quad (16)$$

where $y_c^r = \frac{e^{z_c^r}}{\sum_{c=1}^4 e^{z_c^r}}$ indicates the predicted probability of rotation angle, while \hat{y}_c^r denotes the groundtruth probability. The complete loss in SS-R-Mod is $\mathcal{L}^s + \mathcal{L}^r$.

In the SS-M-Mod, it also uses the standard classification loss, but change the rotation-based self-supervised auxiliary loss to mirror-based self-supervised auxiliary loss \mathcal{L}^m , which can be defined as:

$$\mathcal{L}^m = - \sum_{c=1}^3 \hat{y}_c^m \log(y_c^m) \quad (17)$$

where y_c^m indicates the predicted probability of mirroring way, while \hat{y}_c^m denotes the groundtruth probability. The complete loss in SS-M-Mod is $\mathcal{L}^s + \mathcal{L}^m$.

F. Discussion and Analysis

In this section, we will further discuss and analyze our work from two aspects. We first see the comparison of our Isolated Graph Learning (IGL) with traditional Graph Learning (GL); next conclude with a comprehensive analysis of the reasons for the success of GCT.

1) *Comparison of IGL and GL*: Compared with IGL, the GL's objective function is different, which can be formulated as:

$$\mathcal{F}(\mathbf{R}) = f_4(\mathbf{R}) + \beta f_5(\mathbf{R}) \quad (18)$$

where \mathbf{R} is the to-be-predicted soft label matrix. β denotes the parameter to balance the function. $f_4(\mathbf{R})$ denotes the graph Laplacian regularizer, which can be formulated as:

$$f_4(\mathbf{R}) = \text{tr}(\mathbf{R}^T \Delta \mathbf{R}) \quad (19)$$

where $\Delta = \mathbf{D}^{-\frac{1}{2}} \mathbf{A} \mathbf{D}^{-\frac{1}{2}}$ denotes the normalized graph Laplacian operator. $f_5(\mathbf{R})$ indicates the empirical loss term, which can be formulated as:

$$f_5(\mathbf{R}) = \|\mathbf{R} - \mathbf{Y}\|_F^2 \quad (20)$$

where \mathbf{Y} indicates the initial one-hot label matrix.

Comparing equations 2,3,4 and equations 18,19,20, it can be seen that the most essential difference between IGL and GL is that we replace \mathbf{R} with $\mathbf{X}^T \mathbf{P}$. If directly using \mathbf{R} , the training samples and the to-be-classified testing samples must be employed together to achieve the testing samples' label prediction. In other words, if we only use the training data to construct the graph, we can only achieve label propagation between training samples. When a new batch of testing data arrives, we must rebuild the graph based on the training and testing data to realize the label prediction for the testing samples. While IGL is different. After we get \mathbf{P} based on the training data, we can directly predict the label of new testing data based on \mathbf{P} without rebuilding the graph.

2) *Comprehensive Analysis of GCT*: Here, let's sort out why GCT is effective. After dismantling it, we find that there are three parts that positively influence our method:

(i) The first point is that the base classifier IGL we designed maps the original features to the graph space, which can reduce the dependence on features in the FSL task, thereby weakening the influence of the FEM problem.

(ii) The second point is that we introduce multi-modal information. In the FSL task, the features obtained by different feature extractors are different. Although they all cause the distribution-shift, the angle of shift varies. Through the mutual correction of multi-modal information, the final performance can be improved.

(iii) The third point is that the employed co-training strategy is reasonable and efficient. As mentioned before, we use multi-modal information here. However, multi-modal features are a double-edged sword. If used well, features with different shortcomings can be corrected with each other to improve performance. If used incorrectly, the performance will be further degraded. In the co-training strategy, we select the most confident sample in a single modality (the selected sample can be treated as the one that is not affected by distribution-shift), and then amplify the advantages of each modality through the alternate iterations of the two modalities, so as to enhance the classifier's ability.

V. EXPERIMENTS

In this section, we design experiments to evaluate our method. Specifically, we first illustrate the experimental setup, containing datasets and implementation details. Then, we demonstrate the comparison results and discuss them in detail. Next, we design ablation studies to further analyze our method. In the end, we observe the experimental performances of multi-modal fusion and cross-domain. All experiments are conducted on a Tesla-V100 GPU with 32G memory.

A. Experimental Setup

1) *Datasets*: Our experiments are carried out on five benchmark datasets, including mini-ImageNet [56], tiered-ImageNet [34], CIFAR-FS [33], FC100 [42], and CUB [57]. mini-ImageNet and tiered-ImageNet are selected from the ImageNet dataset [58] and as the subsets. mini-ImageNet consists of 100 classes with 600 images per class, and tiered-ImageNet has 608 classes and each class contains 1,281 images on average. Both of them resize the image to 84×84 . Following the standard split way as [11], for mini-ImageNet, the base set contains 64 selected classes, the validation is composed of 16 classes, and the novel set includes 20 classes. Similarly, for tiered-ImageNet, the base set includes 351 classes, the validation set contains 97 classes, and 160 classes are prepared for the novel set. The CIFAR-FS and FC100 are the subsets of the CIFAR-100 dataset [59], which includes 100 classes. According to the split introduced in [33], CIFAR-FS is divided into 64 classes, and it can be seen as the base set, the validation set consists of 16 classes, and the novel set includes 20 classes. And for FC100, we divided it into 60 classes as the base set, the validation set contains 20 classes, and the novel set includes 20 classes. The image size of CIFAR-FS and FC100 datasets are set to 32×32 . There are 11,788 images with 200 categories in the CUB dataset in total. Referring to the implementation in ICI [11], CUB is divided into 100 classes as the base set, the validation set contains 50 classes, and the novel set consists of 50 classes. In all experiments, the images are cropped into 84×84 .

2) *Implementation Details*: In our paper, both the rotation-modal and mirror-modal feature extractors adopt the ResNet12 [60] backbone, which contains four residual blocks (a convolution layer with 3×3 kernel size, batch normalization layer, and LeakyReLU layer), four 2×2 max-pooling layers, and four dropout layers. The optimizer is adopting stochastic gradient descent (SGD) with Nesterov momentum (0.9). The training epochs are set as 120, and then all module was tested over 600 episodes with 15 query samples per class. For more details of network experimental implements, such as the learning rate, data augmentation, and the number of filters, please refer to ICI [11]. Besides the feature extractor, the designed classifier also affects the final results (*i.e.*, the two parameters in Equation 6). For fairness and convenience, we fix $\lambda = 0.1$ and $\mu = 0.6$ for all the datasets by our empirical tuning. And in Section ??, we discuss the influence of the two parameters.

TABLE II: The 5-way semi-supervised few-shot classification accuracies (%) with 95% confidence intervals over 600 episodes. $(\cdot)^*$, and $(\cdot)^\dagger$ in this table indicate inductive semi-supervised, and transductive semi-supervised settings, respectively. About the influence of the unlabeled number, please see Figure ??.

Method	Venue	Backbone	mini-ImageNet		tiered-ImageNet		CIFAR-FS		FC100	
			1-shot	5-shot	1-shot	5-shot	1-shot	5-shot	1-shot	5-shot
MSkM [34]	ICLR'18	ResNet12	62.10	73.60	68.60	81.00	-	-	-	-
TPN [35]	ICLR'19	ResNet12	62.70	74.20	72.10	83.30	-	-	-	-
LST [10]	NIPS'19	ResNet12	70.10	78.70	77.70	85.20	73.00	85.62	42.77	57.67
EPNet [36]	ECCV'20	ResNet12	75.36	84.07	81.79	88.45	76.77	86.03	45.21	59.81
TransMatch [37]	CVPR'20	ResNet12	63.02	81.19	-	-	-	-	-	-
ICI [11]	CVPR'20	ResNet12	71.41	81.12	85.44	89.12	78.07	84.76	46.27	61.30
PLCM [12]	ICCV'21	ResNet12	72.06	83.71	84.78	90.11	77.62	86.13	48.35	62.75
PTN [38]	AAAI'21	WRN	82.66	<u>88.43</u>	84.70	89.14	-	-	-	-
iLPC [13]	ICCV'21	ResNet12	70.99	81.06	85.04	89.63	78.57	85.84	-	-
MHFC [17]	ACMMM'21	ResNet12	79.26	87.30	<u>87.57</u>	91.80	<u>84.74</u>	90.19	<u>50.95</u>	64.05
GCT*	Ours	ResNet12	78.73	88.57	88.65	91.53	84.91	90.67	52.78	65.21
GCT[†]	Ours	ResNet12	<u>80.04</u>	88.29	88.74	92.07	85.11	91.00	53.64	64.95

TABLE III: The 5-way multi-modal fusion based few-shot classification accuracies (%) with 95% confidence intervals over 600 episodes in mini-ImageNet and tiered-ImageNet. For a fair comparison, the reported results of our GCT is based on the transductive supervised setting.

Method	Backbone	mini-ImageNet		tiered-ImageNet	
		1-shot	5-shot	1-shot	5-shot
DenseCls [22]	ResNet12	62.53	79.77	-	-
DWC [25]	ResNet12	63.73	81.19	70.44	85.43
DivCoop [23]	ResNet12	64.14	81.23	-	-
URT [24]	ResNet12	72.23	83.35	80.30	88.63
MHFC [17]	ResNet12	<u>73.10</u>	81.75	82.10	87.99
GCT	ResNet12	75.29	85.17	86.10	90.18

TABLE IV: The 5-way few-shot classification accuracies (%) with 95% confidence intervals over 600 episodes in CIFAR-FS and FC100. This table compares our GCT with state-of-the-arts without considering any variables, such as backbones, tricks, or even the few-shot settings, just reports the final performances.

Method	Backbone	CIFAR-FS		FC100	
		1-shot	5-shot	1-shot	5-shot
ProtoNet [39]	4CONV	55.50	72.00	35.30	48.600
MAML [40]	4CONV	58.90	71.50	-	-
RelationNet [41]	4CONV	55.00	69.30	-	-
TADAM [42]	ResNet12	-	-	40.10	56.10
DenseCls [22]	ResNet12	-	-	42.04	57.63
MetaOpt [33]	ResNet12	72.00	84.20	41.10	55.50
TEAM [43]	ResNet12	70.43	81.25	-	-
MABAS [44]	ResNet12	73.24	85.65	41.74	57.11
Fine-tuning [45]	WRN	<u>76.58</u>	85.79	<u>43.16</u>	57.57
DSN-MR [46]	ResNet12	75.60	<u>86.20</u>	-	-
GCT	ResNet12	85.11	91.00	53.64	65.21

B. Experimental Results

1) Comparison Results with Semi-Supervised Methods:

Table II shows the comparison results with recently proposed semi-supervised few-shot classification methods. These approaches use the unlabeled samples to correct the distribution. Obviously, our GCT achieves outstanding performances. First

TABLE V: The 5-way few-shot classification accuracies (%) with 95% confidence intervals over 600 episodes in mini-ImageNet and tiered-ImageNet. This table compares our GCT with several state-of-the-arts without considering any variables, such as backbones, tricks, or even the few-shot settings, just reports the final performances.

Method	Backbone	mini-ImageNet		tiered-ImageNet	
		1-shot	5-shot	1-shot	5-shot
ProtoNet [39]	4CONV	49.42	68.20	-	-
MAML [40]	4CONV	48.70	63.11	-	-
RelationNet [41]	ResNet18	52.48	69.83	-	-
Baseline [47]	ResNet18	51.75	74.27	-	-
Baseline++ [47]	ResNet18	51.87	75.68	-	-
LEO [48]	WRN	61.76	77.59	66.33	81.44
TPN [35]	4CONV	52.78	66.42	55.74	71.01
AM3 [49]	ResNet12	65.30	78.10	69.08	82.58
TapNet [50]	ResNet12	61.65	76.36	63.08	80.26
CTM [51]	ResNet18	64.12	80.51	-	-
MetaOpt [33]	ResNet12	62.64	78.63	65.99	81.56
TEAM [43]	ResNet12	60.07	75.90	-	-
S2M2 [16]	WRN	64.93	83.18	73.71	88.59
Fine-tuning [45]	WRN	65.73	78.40	73.34	85.50
DSN-MR [46]	ResNet12	64.60	79.51	67.39	82.85
MABAS [44]	ResNet12	64.21	81.01	-	-
HGNIN [52]	4CONV	60.03	79.64	64.32	83.34
DC [53]	WRN	<u>68.57</u>	82.88	78.19	<u>89.90</u>
ICI [11]	ResNet12	66.80	79.26	<u>80.79</u>	87.92
MELR [54]	ResNet12	67.40	83.40	72.14	87.01
ODE [55]	1	67.76	82.71	71.89	85.96
GCT	ResNet12	80.04	88.57	88.74	92.07

see the comparison without considering PTN [38]. Specifically, in mini-ImageNet, GCT exceeds others 0.78%-17.94% in the 1-shot case, and 1.27%-14.97% in the 5-shot case; in tiered-ImageNet, GCT exceeds others 1.17%-20.14% in the 1-shot case, and 0.27%-11.07% in the 5-shot case; in CIFAR-FS, GCT exceeds others 0.37%-12.11% in the 1-shot case, and 0.81%-6.24% in the 5-shot case; in FC100, GCT exceeds others 2.69%-10.87% in the 1-shot case, 1.16%-7.54% in the 5-shot case. And then comparing GCT with PTN, we find that only in mini-ImageNet, the performance of GCT is slightly inferior to PTN, while in other datasets, GCT is better than PTN.

2) Comparison Results with Multi-Modal Fusion Methods:

Our GCT fuses two modal information, so that it is necessary to compare it with recently proposed multi-modal fusion based methods. The comparison results are presented in Table III. For a fair comparison, we do not utilize the unlabeled data. We exploit our GCT in the transductive setting. We find that our GCT can outperform other methods by 1.82%-12.76% in mini-ImageNet, and 1.55%-15.66% in tiered-ImageNet.

3) Comparison Results with State-of-The-Art Methods:

All the works have their highlights and tricks to improve their final performances. In this section, we compare our GCT with other state-of-the-art methods. That means, we do not consider the impact of any variables, such as backbones, various tricks, or even the few-shot settings (*i.e.*, inductive supervised, transductive supervised, inductive semi-supervised, transductive semi-supervised settings), but only report their final results. From Table V, IV, we observe that, our proposed GCT has achieved significant improvements compared with other SOTAs. In mini-ImageNet dataset, GCT exceeds others at least 11.47% in the 1-shot case, and 5.17% in the 5-shot case. In tiered-ImageNet dataset, GCT outperforms others at least 7.95% in the 1-shot case, and 2.17% in the 5-shot case. In CIFAR-FS dataset, GCT gains improvements of at least 8.53% in the 1-shot case, and 4.52% in the 5-shot case. In FC100 dataset, GCT surpasses others by at least 10.36% in the 1-shot case, and 6.88% in the 5-shot case.

VI. CONCLUSION

There is a fundamental problem in Few-shot learning based tasks, *i.e.*, Feature-Extractor-Maladaptive (FEM) problem. In this paper, we make two efforts to address this challenge. First, we propose a novel label prediction method, Isolated Graph Learning (IGL), to encode the feature embedding to graph representation and then propagate the label information through graph structure for prediction. Second, we extend IGL to the co-training framework to exploit multi-modal features in the semi-supervised setting, dubbed as Graph Co-Training (GCT). From the two perspectives, we have tackled this challenge to some extent. In our future work, we may study to improve the quality of the co-training strategy.

use section* for acknowledgment

ACKNOWLEDGMENT

The paper was supported by the Yunnan Key Laboratory of Media Convergence; the Natural Science Foundation of Shandong Province, China (Grant No. ZR2019MF073); the Open Research Fund from Shandong Provincial Key Laboratory of Computer Network (No. SDKLCN-2018-01); Qingdao Science and Technology Project (No. 17-1-1-8-jch); the Fundamental Research Funds for the Central Universities, China University of Petroleum (East China) (Grant No. 20CX05001A); the Major Scientific and Technological Projects of CNPC (No. ZD2019-183-008); the Creative Research Team of Young Scholars at Universities in Shandong Province (No.2019KJN019), and the Graduate Innovation Project of China University of Petroleum (East China) Grant No. YCX2021123 and No. YCX2021117.

REFERENCES

- [1] S. Shao, L. Xing, R. Xu, W. Liu, Y.-J. Wang, and B.-D. Liu, “Mdflm: Multi-decision fusing model for few-shot learning,” *IEEE Transactions on Circuits and Systems for Video Technology*, 2021.
- [2] K. Wang, D. Zhang, Y. Li, R. Zhang, and L. Lin, “Cost-effective active learning for deep image classification,” *IEEE Transactions on Circuits and Systems for Video Technology*, vol. 27, no. 12, pp. 2591–2600, 2016.
- [3] S. Shao, R. Xu, W. Liu, B.-D. Liu, and Y.-J. Wang, “Label embedded dictionary learning for image classification,” *Neurocomputing*, vol. 385, pp. 122–131, 2020.
- [4] L. Wang, B. Fan, Z. Guo, Y. Zhao, R. Zhang, R. Li, and W. Gong, “Dense-scale feature learning in person re-identification,” in *Asian Conference on Computer Vision*, 2020.
- [5] Z. Zheng, L. Zheng, and Y. Yang, “Pedestrian alignment network for large-scale person re-identification,” *IEEE Transactions on Circuits and Systems for Video Technology*, vol. 29, no. 10, pp. 3037–3045, 2018.
- [6] B. Fan, L. Wang, R. Zhang, Z. Guo, Y. Zhao, R. Li, and W. Gong, “Contextual multi-scale feature learning for person re-identification,” in *ACM International Conference on Multimedia*, 2020, pp. 655–663.
- [7] Y. Wang, Y. Zhao, S. Ying, S. Du, and Y. Gao, “Rotation-invariant point cloud representation for 3-d model recognition,” *IEEE Transactions on Cybernetics*, 2022.
- [8] G. Qian, H. Hammoud, G. Li, A. Thabet, and B. Ghanem, “Assanet: An anisotropic separable set abstraction for efficient point cloud representation learning,” in *Advances in Neural Information Processing Systems*, vol. 34, 2021.
- [9] L. Zhao, K.-K. Ma, Z. Liu, Q. Yin, and J. Chen, “Real-time scene-aware lidar point cloud compression using semantic prior representation,” *IEEE Transactions on Circuits and Systems for Video Technology*, 2022.
- [10] X. Li, Q. Sun, Y. Liu, Q. Zhou, S. Zheng, T.-S. Chua, and B. Schiele, “Learning to self-train for semi-supervised few-shot classification,” in *Neural Information Processing Systems*, vol. 32, 2019, pp. 10 276–10 286.
- [11] Y. Wang, C. Xu, C. Liu, L. Zhang, and Y. Fu, “Instance credibility inference for few-shot learning,” in *Computer Vision and Pattern Recognition*, 2020, pp. 12 836–12 845.
- [12] K. Huang, J. Geng, W. Jiang, X. Deng, and Z. Xu, “Pseudo-loss confidence metric for semi-supervised few-shot learning,” in *International Conference on Computer Vision*, 2021, pp. 8671–8680.
- [13] M. Lazarou, T. Stathaki, and Y. Avrithis, “Iterative label cleaning for transductive and semi-supervised few-shot learning,” in *International Conference on Computer Vision*, 2021, pp. 8751–8760.
- [14] M. Belkin and P. Niyogi, “Laplacian eigenmaps and spectral techniques for embedding and clustering,” in *Neural Information Processing Systems*, 2002, pp. 585–591.
- [15] D. Zhou, O. Bousquet, T. Lal, J. Weston, and B. Schölkopf, “Learning with local and global consistency,” *Neural Information Processing Systems*, vol. 16, pp. 321–328, 2003.
- [16] P. Mangla, N. Kumari, A. Sinha, M. Singh, B. Krishnamurthy, and V. N. Balasubramanian, “Charting the right manifold: Manifold mixup for few-shot learning,” in *IEEE Winter Conference on Applications of Computer Vision*, 2020, pp. 2218–2227.
- [17] S. Shao, L. Xing, Y. Wang, R. Xu, C. Zhao, Y.-J. Wang, and B.-D. Liu, “Mhfc: Multi-head feature collaboration for few-shot learning,” in *ACM International Conference on Multimedia*, 2021.
- [18] Y. Chen, Y. Ma, T. Ko, J. Wang, and Q. Li, “Metamix: Improved meta-learning with interpolation-based consistency regularization,” in *ICPR*, 2020.
- [19] S. Huang, X. Zeng, S. Wu, Z. Yu, M. Azzam, and H.-S. Wong, “Behavior regularized prototypical networks for semi-supervised few-shot image classification,” *Pattern Recognition*, p. 107765, 2020.
- [20] D. Berthelot, N. Carlini, I. Goodfellow, N. Papernot, A. Oliver, and C. A. Raffel, “Mixmatch: A holistic approach to semi-supervised learning,” in *Neural Information Processing Systems*, 2019, pp. 5049–5059.
- [21] K. Sohn, D. Berthelot, C.-L. Li, Z. Zhang, N. Carlini, E. D. Cubuk, A. Kurakin, H. Zhang, and C. Raffel, “Fixmatch: Simplifying semi-supervised learning with consistency and confidence,” in *Neural Information Processing Systems*, 2020.
- [22] Y. Lifchitz, Y. Avrithis, S. Picard, and A. Bursuc, “Dense classification and implanting for few-shot learning,” in *Computer Vision and Pattern Recognition*, 2019, pp. 9258–9267.
- [23] N. Dvornik, C. Schmid, and J. Mairal, “Selecting relevant features from a multi-domain representation for few-shot classification,” in *European Conference on Computer Vision*. Springer, 2020, pp. 769–786.

[24] L. Liu, W. Hamilton, G. Long, J. Jiang, and H. Larochelle, “A universal representation transformer layer for few-shot image classification,” in *International Conference on Learning Representations*, 2021.

[25] N. Dvornik, C. Schmid, and J. Mairal, “Diversity with cooperation: Ensemble methods for few-shot classification,” in *International Conference on Computer Vision*, 2019, pp. 3723–3731.

[26] V. Garcia and J. Bruna, “Few-shot learning with graph neural networks,” in *International Conference on Learning Representations*, 2017.

[27] J. Kim, T. Kim, S. Kim, and C. D. Yoo, “Edge-labeling graph neural network for few-shot learning,” in *Computer Vision and Pattern Recognition*, 2019, pp. 11–20.

[28] L. Yang, L. Li, Z. Zhang, X. Zhou, E. Zhou, and Y. Liu, “Dpgn: Distribution propagation graph network for few-shot learning,” in *Computer Vision and Pattern Recognition*, 2020, pp. 13 390–13 399.

[29] S. Tang, D. Chen, L. Bai, K. Liu, Y. Ge, and W. Ouyang, “Mutual crf-gnn for few-shot learning,” in *Conference on Computer Vision and Pattern Recognition*, 2021, pp. 2329–2339.

[30] L. Yang, D. Chen, X. Zhan, R. Zhao, C.-C. Loy, and D. Lin, “Learning to cluster faces via confidence and connectivity estimation,” in *Conference on Computer Vision and Pattern Recognition*, 2020, pp. 13 369–13 378.

[31] Z. Wang, L. Zheng, Y. Li, and S. Wang, “Linkage based face clustering via graph convolution network,” in *Conference on Computer Vision and Pattern Recognition*, 2019, pp. 1117–1125.

[32] Z. Zhang, H. Lin, X. Zhao, R. Ji, and Y. Gao, “Inductive multi-hypergraph learning and its application on view-based 3d object classification,” *IEEE Transactions on Image Processing*, vol. 27, no. 12, pp. 5957–5968, 2018.

[33] K. Lee, S. Maji, A. Ravichandran, and S. Soatto, “Meta-learning with differentiable convex optimization,” in *Computer Vision and Pattern Recognition*, 2019, pp. 10 657–10 665.

[34] M. Ren, E. Triantafillou, S. Ravi, J. Snell, K. Swersky, J. B. Tenenbaum, H. Larochelle, and R. S. Zemel, “Meta-learning for semi-supervised few-shot classification,” in *International Conference on Learning Representations*, 2018.

[35] Y. Liu, J. Lee, M. Park, S. Kim, E. Yang, S. J. Hwang, and Y. Yang, “Learning to propagate labels: Transductive propagation network for few-shot learning,” in *International Conference on Learning Representations*, 2019.

[36] P. Rodríguez, I. Laradji, A. Drouin, and A. Lacoste, “Embedding propagation: Smoother manifold for few-shot classification,” in *European Conference on Computer Vision*, 2020.

[37] Z. Yu, L. Chen, Z. Cheng, and J. Luo, “Transmatch: A transfer-learning scheme for semi-supervised few-shot learning,” in *Computer Vision and Pattern Recognition*, 2020, pp. 12 856–12 864.

[38] H. Huang, J. Zhang, J. Zhang, Q. Wu, and C. Xu, “Ptn: A poisson transfer network for semi-supervised few-shot learning,” in *AAAI Conference on Artificial Intelligence*, 2021.

[39] J. Snell, K. Swersky, and R. Zemel, “Prototypical networks for few-shot learning,” in *Neural Information Processing Systems*, 2017, pp. 4077–4087.

[40] C. Finn, P. Abbeel, and S. Levine, “Model-agnostic meta-learning for fast adaptation of deep networks,” in *International Conference on Machine Learning*, 2017, pp. 1126–1135.

[41] F. Sung, Y. Yang, L. Zhang, T. Xiang, P. H. Torr, and T. M. Hospedales, “Learning to compare: Relation network for few-shot learning,” in *Computer Vision and Pattern Recognition*, 2018, pp. 1199–1208.

[42] B. Oreshkin, P. R. López, and A. Lacoste, “Tadam: Task dependent adaptive metric for improved few-shot learning,” in *Neural Information Processing Systems*, 2018, pp. 721–731.

[43] L. Qiao, Y. Shi, J. Li, Y. Wang, T. Huang, and Y. Tian, “Transductive episodic-wise adaptive metric for few-shot learning,” in *International Conference on Computer Vision*, 2019, pp. 3603–3612.

[44] J. Kim, H. Kim, and G. Kim, “Model-agnostic boundary-adversarial sampling for test-time generalization in few-shot learning,” *European Conference on Computer Vision*, pp. 599–617, 2020.

[45] G. S. Dhillon, P. Chaudhari, A. Ravichandran, and S. Soatto, “A baseline for few-shot image classification,” in *International Conference on Learning Representations*, 2020.

[46] C. Simon, P. Koniusz, R. Nock, and M. Harandi, “Adaptive subspaces for few-shot learning,” in *Computer Vision and Pattern Recognition*, 2020, pp. 4136–4145.

[47] W.-Y. Chen, Y.-C. Liu, Z. Kira, Y.-C. F. Wang, and J.-B. Huang, “A closer look at few-shot classification,” in *International Conference on Learning Representations*, 2019.

[48] A. A. Rusu, D. Rao, J. Sygnowski, O. Vinyals, R. Pascanu, S. Osindero, and R. Hadsell, “Meta-learning with latent embedding optimization,” in *International Conference on Learning Representations*, 2019.

[49] C. Xing, N. Rostamzadeh, B. Oreshkin, and P. O. Pinheiro, “Adaptive cross-modal few-shot learning,” in *Neural Information Processing Systems*, 2019, pp. 4847–4857.

[50] S. W. Yoon, J. Seo, and J. Moon, “Tapnet: Neural network augmented with task-adaptive projection for few-shot learning,” in *International Conference on Machine Learning*, 2019, pp. 7115–7123.

[51] H. Li, D. Eigen, S. Dodge, M. Zeiler, and X. Wang, “Finding task-relevant features for few-shot learning by category traversal,” in *Computer Vision and Pattern Recognition*, 2019, pp. 1–10.

[52] C. Chen, K. Li, W. Wei, J. T. Zhou, and Z. Zeng, “Hierarchical graph neural networks for few-shot learning,” *IEEE Transactions on Circuits and Systems for Video Technology*, 2021.

[53] S. Yang, L. Liu, and M. Xu, “Free lunch for few-shot learning: Distribution calibration,” in *International Conference on Learning Representations*, 2021.

[54] N. Fei, Z. Lu, T. Xiang, and S. Huang, “Mclr: Meta-learning via modeling episode-level relationships for few-shot learning,” in *International Conference on Learning Representations*, 2021.

[55] C. Xu, C. Liu, L. Zhang, C. Wang, J. Li, F. Huang, X. Xue, and Y. Fu, “Learning dynamic alignment via meta-filter for few-shot learning,” in *Computer Vision and Pattern Recognition*, 2021.

[56] O. Vinyals, C. Blundell, T. Lillicrap, D. Wierstra *et al.*, “Matching networks for one shot learning,” in *Neural Information Processing Systems*, vol. 29, 2016, pp. 3630–3638.

[57] C. Wah, S. Branson, P. Welinder, P. Perona, and S. Belongie, “The caltech-ucsd birds-200-2011 dataset,” 2011.

[58] O. Russakovsky, J. Deng, H. Su, J. Krause, S. Satheesh, S. Ma, Z. Huang, A. Karpathy, A. Khosla, M. Bernstein *et al.*, “Imagenet large scale visual recognition challenge,” *International Journal of Computer Vision*, vol. 115, no. 3, pp. 211–252, 2015.

[59] A. Krizhevsky, G. Hinton *et al.*, “Learning multiple layers of features from tiny images,” *Computer Science Department, University of Toronto*, 2009.

[60] K. He, X. Zhang, S. Ren, and J. Sun, “Deep residual learning for image recognition,” in *Computer Vision and Pattern Recognition*, 2016, pp. 770–778.